Adaptive Attitude Control of a Rigid Body with Input and Output Quantization

Siri Marte Schlanbusch[1], Jing Zhou[1] and Rune Schlanbusch[2]

[1]Department of Engineering Sciences
University of Agder
4879 Grimstad, Norway

[2]Norwegian Research Centre AS
4879 Grimstad, Norway

Abstract

In this article, the adaptive attitude-tracking problem of a rigid body is investigated, where the input and output are transmitted via a network. To reduce the communication burden in a network, a quantizer is introduced in both uplink and downlink communication channels. An adaptive backstepping-based control scheme is developed for a class of multiple-input and multiple-output (MIMO) rigid body systems. The proposed control algorithm can overcome the difficulty to proceed with the recursive design of virtual controls with quantized output vector and a new approach to stability analysis is developed by constructing a new compensation scheme for the effects of the vector output quantization and input quantization. It is shown that all closed-loop signals are ensured uniformly bounded and the tracking errors converge to a compact set containing the origin. Experiments on a 2 degrees-of-freedom helicopter system illustrate the effectiveness of the proposed control scheme.

Nomenclature

$d_{(\cdot)}$	Quantization error related to $(\cdot)$.
$\boldsymbol{e}$	Tracking error, quaternion.
$\boldsymbol{f}_g^i$	Gravitational force, expressed in i frame.
g	Gravitational acceleration.
$\boldsymbol{g}(\boldsymbol{q})$	Moment caused by the gravitational force.
$\boldsymbol{G}$	Error kinematics matrix.

$\boldsymbol{I}$ Identity matrix.

$\boldsymbol{J}$ Inertia matrix about the origin o, decomposed in the b frame.

$k_{(\cdot)}$ Positive constant related to $(\cdot)$.

$\boldsymbol{k}$ Euler axis.

l Length of quantization interval.

m Mass of the rigid body.

$\boldsymbol{q}$ Attitude.

$\boldsymbol{q}_{a,b}$ Unit quaternion $\boldsymbol{q}$ in b frame relative to a frame.

$\boldsymbol{r}_g^b$ Distance from the origin to the center of mass, decomposed in the b frame.

$\boldsymbol{R}_a^b$ Rotation matrix from frame a to frame b.

R Number of bits.

$\boldsymbol{S}(\boldsymbol{a})\boldsymbol{b}$ Cross product operator $\times$ between two vectors $\boldsymbol{a}$ and $\boldsymbol{b}$, where $\boldsymbol{S}$ is skew-symmetric.

$\boldsymbol{T}, \boldsymbol{\Psi}, \boldsymbol{\Phi}$ Known nonlinear functions of $\boldsymbol{q}$ and $\boldsymbol{\omega}$.

$\boldsymbol{u}$ Control input.

V Lyapunov function candidate.

$\boldsymbol{\tau}_d$ External disturbance.

$\delta_{(\cdot)}$ Maximum bounded value for $d_{(\cdot)}$.

$\boldsymbol{\varepsilon}$ Imaginary parts of a unit quaternion.

η Real part of a unit quaternion.

$\boldsymbol{\theta}$ Unknown constant vector.

$\lambda_{\max}(\cdot)$ Maximum eigenvalue of the matrix $(\cdot)$.

$\lambda_{\min}(\cdot)$ Minimum eigenvalue of the matrix $(\cdot)$.

υ Euler angle.

$\boldsymbol{\omega}$ Angular velocity.

$\boldsymbol{\omega}_{b,a}^c$ Angular velocity of frame a relative to frame b, expressed in frame c.

$\mathbb{R}^n$ Set of real numbers, dimension n.

$\mathbb{S}^3$ The non-Euclidean three-sphere.

$(\cdot)^{\mathcal{Q}}$ Quantized signal of $(\cdot)$.

$\|\cdot\|$ The $\mathcal{L}_2$-norm and induced $\mathcal{L}_2$-norm for vectors and matrices, respectively.

Vectors are denoted by small bold letters and matrices with capitalized bold letters.

C.1 Introduction

Attitude control of rigid bodies has been widely addressed in the literature, see e.g. [1–9], and with applications in marine systems in [10], unmanned aerial vehicles (UAVs) in [11], helicopters in [12], underwater vehicles in [13], and other robotic systems. Rigid body systems are utilized in numerous important applications such as transportation [14], inspection [15], search and rescue [16] and remote sensing [17]. In [6], a robust adaptive controller is proposed for the attitude tracking problem of rigid bodies in the presence of uncertain parameters and where the attitude is represented by rotation matrices. In [7], an adaptive attitude tracking controller is developed for rigid body systems in the presence of unknown inertia and gyro-bias. In [8], an adaptive controller is proposed for a leader-following attitude consensus problem for multiple rigid body systems subject to jointly connected switching networks in the presence of uncertain parameters. In [9], an adaptive backstepping controller is proposed for the trajectory tracking of a rigid body with unknown mass and inertia based on dual-quaternions. Chen *et al.* [11] proposed a robust nonlinear controller for quadrotor UAVs, which combines the sliding-mode control technique and the backstepping control technique. In [12], adaptive backstepping control is proposed for pitch and yaw control of a 2 degrees-of-freedom (DOF) helicopter system. Yan and Yu [13] investigated the sliding mode tracking control of underwater vehicles.

Quantized control has attracted considerable attention in recent years, due to its theoretical and practical importance in practical engineering, where digital processors are widespread used and signals are required to be quantized and transmitted via a common network to reduce the communication burden. However, most of the works on quantized feedback control are concerned with either input quantization [18–25] or state quantization [26, 27].

In practice, it is common that both the inputs and the states of rigid bodies are quantized due to actuator and sensor limitations. Control of rigid bodies with quantized signals is a potential problem and has received attention with a demand on stability and reliability. For example, the remote control of a group of vehicles or robots, where the signals are transmitted over a shared network using quantization

techniques. Attitude stabilization with input quantization is investigated in [28] using a fixed-time sliding mode control. Trajectory tracking control for autonomous underwater vehicles with the effect of quantization is investigated in [13] using a sliding mode controller, where the considered systems are completely known. In [29], adaptive tracking control is proposed for underactuated autonomous underwater vehicles with input quantization.

Uncertainties and non-linearities always exist in many practical systems. Research on adaptive control of rigid bodies with either input quantization or state quantization using backstepping technique has received attention, see for examples, [29–31]. In [30], an adaptive backstepping control scheme with quantized inputs is presented for a 2 DOF helicopter system, considering a uniform quantizer. In [29], adaptive backstepping is investigated for tracking control for under-actuated autonomous underwater vehicles with input quantization. An adaptive backstepping controller is proposed for formation tracking control for a group of UAVs with quantized inputs in [31]. Actually, the above cited attitude control approaches do not consider the problem which takes both the input quantization and state quantization into account.

In this article, we aim to solve the attitude tracking of uncertain nonlinear rigid body systems with both input and output quantization. The system is modeled as a nonlinear multiple-input-multiple-output (MIMO) system, with challenges in controller design due to its nonlinear behavior, its cross coupling effect between inputs and outputs, and with uncertainties both in the model and the parameters. A uniform quantization is used for signals in order to reduce the communication burden. A new backstepping based adaptive controller and a new approach to stability analysis are proposed. The full state vector is considered in the stability, that is often forgotten for quaternion based attitude control, where the scalar part of the quaternion is left out. The proposed method is tested on a 2 DOF helicopter system from Quanser. It is analytically shown how the choice of quantization level affects the tracking performance, where a higher quantization level increases the tracking error. The experiments on the helicopter system illustrate the proposed scheme.

With aforementioned features, the main contributions of this paper are summarized as follows.

- As far as we are concerned, this is the first work which solves the adaptive control problem for rigid body systems with unknown parameters and with both input and output quantization, where a bounded type of quantizer is considered, meanwhile guaranteeing that the attitude error and velocity error will converge to a compact set. Compared with [24] where only input quantization is considered, and [27] where only state quantization is considered, this research studies both input and output quantization problem. The main challenge is that

the designed controller and virtual controls can only utilize quantized states and both the effects of input and output quantization introduce numerous residual terms that need to be dominated. Additionally, the quantization causes discrete phenomenons which complicates the controller design and stability analysis. To overcome this difficulty, differentiable virtual controls are firstly designed by assuming that the system has no quantization. Their partial derivatives multiplied by the quantized signals are then utilized to complete the design of virtual controls for the case with quantized input and output.

- Compared to backstepping control of single-input-single-output (SISO) systems with either input or state quantization in [23–25, 27, 32], this paper considers MIMO uncertain systems with both input and output quantization. The challenge is that the control problem becomes more complicated for MIMO systems due to the coupling among various inputs and outputs. It becomes even more difficult to deal with when there exist uncertain parameters in the coupling matrix and both inputs and outputs are quantized. To overcome the difficulty, a new backstepping based adaptive controller and a new approach to stability analysis are proposed, where the effects of both output and input quantization are compensated for.

C.2 Rigid Body Dynamical Model and Problem Formulation

C.2.1 Attitude Dynamics

The attitude of a rigid body can be represented by e.g. Euler angles in [13, 30], (modified) Rodrigues parameters, rotation matrices in [3, 6] or quaternions in [4, 7, 9], where each representation has different properties. Any three-parameter representations have some kind of singularity, where e.g. Euler angles (roll-pitch-yaw) have kinematic singularities since it is not possible to describe the angular velocity for all angles, and with the potential problem of gimbal lock. Practical applications are often represented by unit quaternions, since this has a nonsingular parameterization. With a desire of a singularity-free representation of the attitude, which is important for agile systems, unit quaternions are used in this paper.

We describe the orientation of a rigid body in the body frame b, relative to an inertial frame i, by a unit quaternion, $\boldsymbol{q} = [\eta, \varepsilon_1, \varepsilon_2, \varepsilon_3]^\top = [\eta, \boldsymbol{\varepsilon}^\top]^\top \in \mathbb{S}^3 = \{x \in \mathbb{R}^4 : \boldsymbol{x}^\top \boldsymbol{x} = 1\}$, that is a complex number, where $\eta = \cos(\upsilon/2) \in \mathbb{R}$ and $\boldsymbol{\varepsilon} = \boldsymbol{k} \sin(\upsilon/2) \in \mathbb{R}^3$. Considering a fully actuated rigid body, the equations of

motion for the attitude dynamics are defined as

$$\dot{\boldsymbol{q}} = \boldsymbol{T}(\boldsymbol{q})\boldsymbol{\omega}, \tag{C.1}$$

$$\boldsymbol{J}\dot{\boldsymbol{\omega}} = \boldsymbol{\Psi}(\boldsymbol{q},\boldsymbol{\omega}) + \boldsymbol{\Phi}(\boldsymbol{\omega})\boldsymbol{\theta} + \boldsymbol{B}\boldsymbol{u}, \tag{C.2}$$

where the angular velocity $\boldsymbol{\omega}_{i,b}^{b} = \boldsymbol{\omega} \in \mathbb{R}^3$, the inertia matrix $\boldsymbol{J} = \mathrm{diag}(J_x, J_y, J_z) \in \mathbb{R}^{3\times3}$ and is positive definite, the unknown constant vector $\boldsymbol{\theta} \in \mathbb{R}^3$, the control allocation matrix $\boldsymbol{B} \in \mathbb{R}^{3\times3}$, the control input $\boldsymbol{u} \in \mathbb{R}^3$, and where

$$\boldsymbol{T}(\boldsymbol{q}) = \frac{1}{2}\begin{bmatrix} -\boldsymbol{\varepsilon}^\top \\ \eta\boldsymbol{I} + \boldsymbol{S}(\boldsymbol{\varepsilon}) \end{bmatrix} \in \mathbb{R}^{4\times3}, \tag{C.3}$$

$$\boldsymbol{\Psi}(\boldsymbol{q},\boldsymbol{\omega}) = -\boldsymbol{S}(\boldsymbol{\omega})(\boldsymbol{J}\boldsymbol{\omega}) - \boldsymbol{g}(\boldsymbol{q}) \ \in \mathbb{R}^3, \tag{C.4}$$

$$\boldsymbol{\Phi}(\boldsymbol{\omega}) = \mathrm{diag}(-\boldsymbol{\omega}) \ \in \mathbb{R}^{3\times3}, \tag{C.5}$$

$$\boldsymbol{g}(\boldsymbol{q}) = -\boldsymbol{S}(\boldsymbol{r}_g^b)\boldsymbol{R}_i^b\boldsymbol{f}_g^i, \tag{C.6}$$

where $\boldsymbol{f}_g^i = [0\ 0\ -mg]^\top$, and the matrix $\boldsymbol{S}(\cdot)$ is the skew-symmetric matrix given by

$$\boldsymbol{S}(\boldsymbol{\varepsilon}) = \begin{bmatrix} 0 & -\varepsilon_3 & \varepsilon_2 \\ \varepsilon_3 & 0 & -\varepsilon_1 \\ -\varepsilon_2 & \varepsilon_1 & 0 \end{bmatrix}. \tag{C.7}$$

If $\boldsymbol{r}_g^b = \boldsymbol{0} \implies \boldsymbol{g(q)} = 0$ and the rotation is about the center of mass. In applications, such as underwater vehicle dynamics, the equations of motion is described by a rotation about a point o, that is not the center of mass [33].
The orientation between two frames can be described by a rotation matrix given as

$$\boldsymbol{R}(\boldsymbol{q}) = \boldsymbol{I} + 2\eta\boldsymbol{S}(\boldsymbol{\varepsilon}) + 2\boldsymbol{S}^2(\boldsymbol{\varepsilon}), \tag{C.8}$$

and the rotation matrix $\boldsymbol{R} \in SO(3)$ that is a special orthogonal group of order 3, and has the property

$$SO(3) = \{\boldsymbol{R} \in \mathbb{R}^{3\times3} : \boldsymbol{R}^\top\boldsymbol{R} = \boldsymbol{I}, \det(\boldsymbol{R}) = 1\}. \tag{C.9}$$

The derivative of a rotation matrix can be expressed as [33]

$$\dot{\boldsymbol{R}}_b^a = \boldsymbol{R}_b^a\boldsymbol{S}(\boldsymbol{\omega}_{a,b}^b) = \boldsymbol{S}(\boldsymbol{\omega}_{a,b}^a)\boldsymbol{R}_b^a. \tag{C.10}$$

Attitude and angular velocities are assumed to be measurable after quantization, and for the control allocation matrix it is assumed that $\det(\boldsymbol{B}) \neq 0$, i.e. the matrix is invertible.

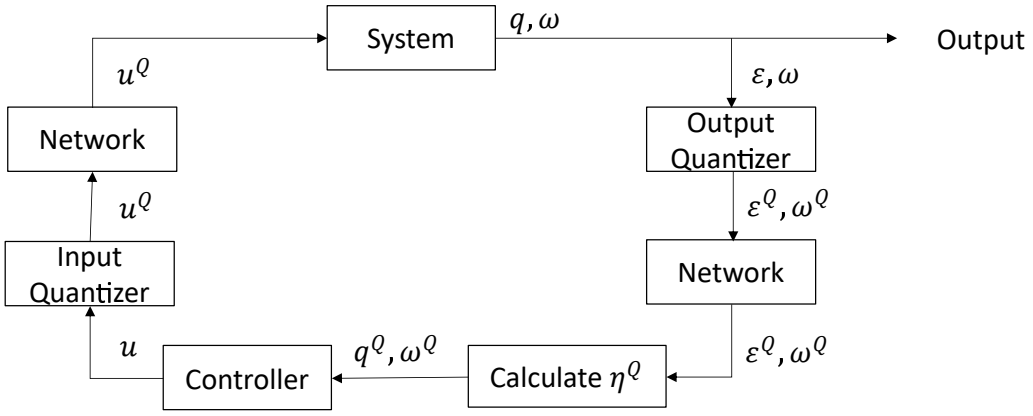

Figure C.1: Control system with quantization over a network.

C.2.2 Problem Statement

We consider a control system as shown in Fig. C.1, where the outputs $\boldsymbol{\varepsilon}, \boldsymbol{\omega}$ and input $\boldsymbol{u}$ are quantized at the encoder side to be sent over the network. It is noted that $\boldsymbol{q} = [\eta, \boldsymbol{\varepsilon}^\top]^\top$. To reduce the communication burden, we have limited the feedback part of the quaternion to only contain $\boldsymbol{\varepsilon}$, as η can be reconstructed due to the unity of the quaternion. The network is assumed noiseless, so that the quantized output signals $\boldsymbol{\varepsilon}^Q, \boldsymbol{\omega}^Q$ are recovered and sent to the controller, and the quantized input signal $\boldsymbol{u}^Q(t)$ is recovered and sent to the plant.

Only the quantized output $\boldsymbol{\varepsilon}^Q, \boldsymbol{\omega}^Q$ are measured, and the quantized value of η is calculated as

$$\eta^Q = \pm\sqrt{1 - (\boldsymbol{\varepsilon}^Q)^\top \boldsymbol{\varepsilon}^Q}, \tag{C.11}$$

to ensure that the property of unit quaternion, $(\boldsymbol{q}^Q)^\top \boldsymbol{q}^Q = 1$, is fulfilled, where the quantized attitude is given by $\boldsymbol{q}^Q = [\eta^Q, (\boldsymbol{\varepsilon}^Q)^\top]^\top$.

Remark 1. *If the state variable η is quantized and sent over the network, we can not ensure that $\boldsymbol{q}^Q$ is a unit quaternion, and a correction/scaling will be needed to ensure this. Since η^Q can be calculated based on the value of $\boldsymbol{\varepsilon}^Q$ and knowledge of the sign of $\eta(t_0)$ and the assumption of sign continuity of $\eta(t)$ based on derivative, we can do the calculation after the network communication. This will also save bandwidth by sending less data over the network.*

Remark 2. *If we are close to, or at $\eta = 0$, we might end up with $(\boldsymbol{\varepsilon}^Q)^\top \boldsymbol{\varepsilon}^Q > 1$, and a scaling is needed to ensure we have a unit quaternion.*

Let $\boldsymbol{q}_{i,d} = \boldsymbol{q}_d$, $\boldsymbol{\omega}^i_{i,d} = \boldsymbol{\omega}_d$, be the desired attitude and angular velocity. The control objective is to design a control law for $\boldsymbol{u}(t) = \boldsymbol{u}(\boldsymbol{q}^Q, \boldsymbol{\omega}^Q)$ by utilizing only quantized outputs $\boldsymbol{q}^Q(t)$ and $\boldsymbol{\omega}^Q(t)$ to ensure that $\boldsymbol{q}^Q(t) \to \boldsymbol{q}_d(t)$ and $\boldsymbol{\omega}^Q(t) \to \boldsymbol{\omega}^Q_{i,d}(t)$

as $t \to \infty$, where the kinematic equation

$$\dot{\boldsymbol{q}}_d = \boldsymbol{T}(\boldsymbol{q}_d)\boldsymbol{\omega}_{i,d}^d = \frac{1}{2}\begin{bmatrix} -\boldsymbol{\varepsilon}_d^\top \\ \eta_d \boldsymbol{I} - \boldsymbol{S}(\boldsymbol{\varepsilon}_d) \end{bmatrix} \boldsymbol{\omega}_d, \tag{C.12}$$

is satisfied, and where all the signals in the closed-loop system are uniformly bounded. To achieve the objective, the following assumptions are imposed.

Assumption 1. *The desired attitude $\boldsymbol{q}_d(t)$, the desired angular velocity $\boldsymbol{\omega}_d(t)$ and the desired angular acceleration $\dot{\boldsymbol{\omega}}_d(t)$ are known, piecewise continuous and bounded functions, that is, there exist $k_{\omega_d}, k_{\dot{\omega}_d} > 0$ such that $\|\boldsymbol{\omega}_d(t)\| < k_{\omega_d}$ and $\|\dot{\boldsymbol{\omega}}_d(t)\| < k_{\dot{\omega}_d}$ $\forall t \geq t_0$.*

Assumption 2. *The unknown parameter vector $\boldsymbol{\theta}$ is bounded by $\|\boldsymbol{\theta}\| \leq k_\theta$, where k_θ is a positive constant. Also $\boldsymbol{\theta} \in C_\theta$, where C_θ is a known compact convex set.*

C.2.3 Quantizer

The quantizer considered in this paper has the following property

$$|y^Q - y| \leq \delta_y, \tag{C.13}$$

where y is a scalar signal and $\delta_y > 0$ denotes the quantization bound. A uniform quantizer is chosen, which has intervals of fixed length and is defined as follows:

$$y^Q = \begin{cases} y_i \operatorname{sgn}(y), & y_i - \frac{l}{2} < |y| \leq y_i + \frac{l}{2} \\ 0, & |y| \leq y_0 \end{cases}, \tag{C.14}$$

where $y_0 > 0, y_1 = y_0 + \frac{l}{2}$, $y_{i+1} = y_i + l$, $l > 0$ is the length of the quantization interval, $\operatorname{sgn}(y)$ is the sign function. The uniform quantization $y^Q \in U = \{0, \pm y_i\}$, and a map of the quantization for $y_i > 0$ is shown in Fig. C.2. Clearly, the property in (C.13) is satisfied with $\delta_y = \max\{y_0, \frac{l}{2}\}$.

When a vector is quantized, we have

$$\boldsymbol{y}^Q = \begin{bmatrix} y_1^Q & y_2^Q & \cdots & y_n^Q \end{bmatrix}^\top, \tag{C.15}$$

and so each vector element is bounded by (C.13), and we have $\|\boldsymbol{y}^Q - \boldsymbol{y}\| = \|\boldsymbol{d}_y\| \leq \|\boldsymbol{\delta}_y\| \triangleq \delta_y$.

Other bounded quantizers such as hysteresis-uniform quantizer and logarithmic-uniform quantizer as presented in [27] can also be considered.

Remark 3. *Communication in a network only has to occur when the quantization levels change. Thus, a higher value for length of the quantization intervals requires less data transmission.*

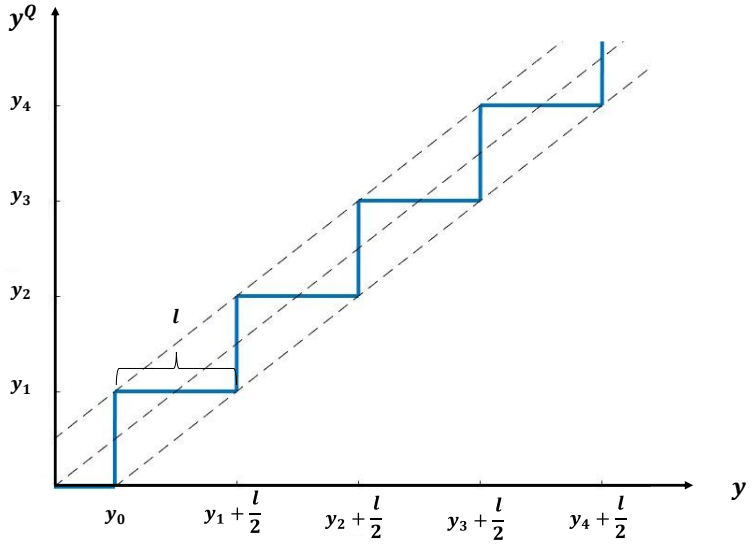

Figure C.2: Map of the uniform quantizer for $y > 0$.

C.3 Controller Design

In this section we will design adaptive feedback control laws for the rigid body using backstepping technique.

C.3.1 Without Quantization

We first consider the case that the output and input are not quantized. For our model, two steps are included, where the control signal is designed in the last step. We begin with a change of coordinates to the error variables. The tracking error $\boldsymbol{e}$ is defined by the quaternion product

$$\boldsymbol{e} = \bar{\boldsymbol{q}}_{i,d} \otimes \boldsymbol{q}_{i,b} = \begin{bmatrix} \tilde{\eta} \\ \tilde{\boldsymbol{\varepsilon}} \end{bmatrix} = \begin{bmatrix} \eta_d \eta + \boldsymbol{\varepsilon}_d^\top \boldsymbol{\varepsilon} \\ \eta_d \boldsymbol{\varepsilon} - \eta \boldsymbol{\varepsilon}_d - S(\boldsymbol{\varepsilon}_d)\boldsymbol{\varepsilon} \end{bmatrix} \in \mathbb{S}^3, \tag{C.16}$$

where $\bar{\boldsymbol{q}} = [\eta \ \ -\boldsymbol{\varepsilon}^\top]^\top$ is the inverse rotation given by the complex conjugate. If $\boldsymbol{q}_{i,b} = \boldsymbol{q}_{i,d}$ then $\boldsymbol{e} = [\pm 1 \ \mathbf{0}_3^\top]^\top$, where $\mathbf{0}_3^\top$ is the zero vector of dimension three. Because there exist two different equilibria using quaternion coordinates, global stability can not be achieved, even though $\boldsymbol{e}$ and $-\boldsymbol{e}$ represent the same physical attitude [2]. We include one further assumption as follows.

Assumption 3. *We assume that* $\operatorname{sgn}(\tilde{\eta}(t_0)) = \operatorname{sgn}(\tilde{\eta}(t)) \ \ \forall t \geq t_0$.

Remark 4. *Assumption 3 is imposed to avoid the problem when the attitude error is close to* $E = \{\boldsymbol{e} \in \mathbb{S}^3 \ : \ \tilde{\eta} = 0\}$.

The relative error kinematics is

$$\dot{\boldsymbol{e}} = \boldsymbol{T}(\boldsymbol{e})\boldsymbol{\omega}_e, \tag{C.17}$$

where $\boldsymbol{T}(\cdot)$ is defined in (C.3) and the angular velocity error is

$$\boldsymbol{\omega}_e = \boldsymbol{\omega} - \boldsymbol{R}_i^b \boldsymbol{\omega}_d. \tag{C.18}$$

Following the backstepping design procedure, the change of coordinates are introduced as

$$\boldsymbol{z}_{1\pm} = \begin{bmatrix} 1 \mp \tilde{\eta} \\ \tilde{\boldsymbol{\varepsilon}} \end{bmatrix}, \quad \boldsymbol{z}_2 = \boldsymbol{\omega}_e - \boldsymbol{\alpha}, \tag{C.19}$$

where $\boldsymbol{z}_{1+}$ is the equilibrium point when $\tilde{\eta}(t_0) \geq 0$ and $\boldsymbol{z}_{1-}$ is the equilibrium point when $\tilde{\eta}(t_0) < 0$ and where $\boldsymbol{\alpha}$ is a virtual controller designed in step 1 as

$$\boldsymbol{\alpha} = -\boldsymbol{C}_1 \boldsymbol{G} \boldsymbol{z}_{1\pm}, \tag{C.20}$$

where $\boldsymbol{C}_1 \in \mathbb{R}^{3\times 3}$ is a positive definite matrix and

$$\begin{aligned} \boldsymbol{G}(\boldsymbol{e})^\top &\triangleq \begin{bmatrix} \pm\tilde{\boldsymbol{\varepsilon}}^\top \\ \tilde{\eta}\boldsymbol{I} + \boldsymbol{S}(\tilde{\boldsymbol{\varepsilon}}) \end{bmatrix} \in \mathbb{R}^{4\times 3}, \\ \dot{\boldsymbol{z}}_{1\pm} &= \frac{1}{2}\boldsymbol{G}^\top \boldsymbol{\omega}_e = -\frac{1}{2}\boldsymbol{G}^\top \boldsymbol{C}_1 \boldsymbol{G} \boldsymbol{z}_{1\pm} + \frac{1}{2}\boldsymbol{G}^\top \boldsymbol{z}_2. \end{aligned} \tag{C.21}$$

For ease of notation we denote $\boldsymbol{z}_1 = \boldsymbol{z}_{1\pm}$ further in the paper. In step 2, the final controller $\boldsymbol{u}(t)$ and parameter update law $\dot{\hat{\boldsymbol{\theta}}}$ are designed as

$$\boldsymbol{u} = \boldsymbol{B}^{-1}\Big[-\boldsymbol{G}\boldsymbol{z}_1 - \boldsymbol{C}_2\boldsymbol{z}_2 - \boldsymbol{\Phi}\hat{\boldsymbol{\theta}} - \boldsymbol{\Psi} - \boldsymbol{J}\Big(\boldsymbol{S}(\boldsymbol{\omega})\boldsymbol{R}_i^b\boldsymbol{\omega}_d - \boldsymbol{R}_i^b\dot{\boldsymbol{\omega}}_d - \dot{\boldsymbol{\alpha}}\Big)\Big], \tag{C.22}$$

$$\dot{\hat{\boldsymbol{\theta}}} = \boldsymbol{\Gamma}\boldsymbol{\Phi}\boldsymbol{z}_2, \tag{C.23}$$

where $\boldsymbol{C}_2 \in \mathbb{R}^{3\times 3}$ and $\boldsymbol{\Gamma} \in \mathbb{R}^{3\times 3}$ are positive definite matrices. We choose a Lyapunov function candidate as

$$V(\boldsymbol{z}_1, \boldsymbol{z}_2, \tilde{\boldsymbol{\theta}}, t) = \boldsymbol{z}_1^\top \boldsymbol{z}_1 + \frac{1}{2}\boldsymbol{z}_2^\top \boldsymbol{J}\boldsymbol{z}_2 + \frac{1}{2}\tilde{\boldsymbol{\theta}}^\top \boldsymbol{\Gamma}^{-1}\tilde{\boldsymbol{\theta}}, \tag{C.24}$$

where $\hat{\boldsymbol{\theta}}$ is the estimated value of $\boldsymbol{\theta}$, and the unknown parameter error is $\tilde{\boldsymbol{\theta}} = \boldsymbol{\theta} - \hat{\boldsymbol{\theta}}$. The derivative of V can be computed as

$$\begin{aligned} \dot{V} = {} & \boldsymbol{z}_1^\top \boldsymbol{G}^\top \boldsymbol{z}_2 - \boldsymbol{z}_1^\top \boldsymbol{G}^\top \boldsymbol{C}_1 \boldsymbol{G}\boldsymbol{z}_1 + \boldsymbol{z}_2^\top \Big[\boldsymbol{\Phi}\boldsymbol{\theta} + \boldsymbol{\Psi} + \boldsymbol{B}\boldsymbol{u} + \boldsymbol{J}\Big(\boldsymbol{S}(\boldsymbol{\omega})\boldsymbol{R}_i^b\boldsymbol{\omega}_d - \boldsymbol{R}_i^b\dot{\boldsymbol{\omega}}_d - \dot{\boldsymbol{\alpha}}\Big)\Big] \\ & - \tilde{\boldsymbol{\theta}}^\top \boldsymbol{\Gamma}^{-1}\dot{\hat{\boldsymbol{\theta}}} \end{aligned}$$

$$= -\boldsymbol{z}_1^\top \boldsymbol{G}^\top \boldsymbol{C}_1 \boldsymbol{G} \boldsymbol{z}_1 - \boldsymbol{z}_2^\top \boldsymbol{C}_2 \boldsymbol{z}_2. \tag{C.25}$$

By applying the LaSalle-Yoshizawa theorem [34], it follows that all signals are uniformly bounded and asymptotic tracking is achieved as $(\boldsymbol{z}_1(t), \boldsymbol{z}_2(t)) \to (\boldsymbol{0}, \boldsymbol{0})$ as $t \to \infty$. The angular velocity error and the angular velocity are bounded by

$$\begin{aligned} \|\boldsymbol{\omega}_e\| &\le \|\boldsymbol{z}_2\| + \lambda_{\max}(\boldsymbol{C}_1)\|\boldsymbol{G}\|\|\boldsymbol{z}_1\| \le \Big[1 + \lambda_{\max}(\boldsymbol{C}_1)\Big]\|\boldsymbol{z}\| \\ &\triangleq k_{\omega_e}\|\boldsymbol{z}\|, \end{aligned} \tag{C.26}$$

$$\begin{aligned} \|\boldsymbol{\omega}\| &\le \|\boldsymbol{\omega}_e + \boldsymbol{R}_i^b \boldsymbol{\omega}_d\| \le k_{\omega_e}\|\boldsymbol{z}\| + \|\boldsymbol{R}_i^b\|\|\boldsymbol{\omega}_d\| \\ &\le k_{\omega_e}\|\boldsymbol{z}\| + k_{\omega_d}, \end{aligned} \tag{C.27}$$

where $\boldsymbol{z} = [\boldsymbol{z}_1^\top, \boldsymbol{z}_2^\top]^\top$.

C.3.2 Quantized Input and Output

When the outputs $\boldsymbol{\varepsilon}$ and $\boldsymbol{\omega}$ and input $\boldsymbol{u}$ are quantized with the property (C.13), we have

$$|{\varepsilon_k}^Q - \varepsilon_k| \le \delta_{\varepsilon_k},\ k = 1, 2, 3, \tag{C.28}$$

$$|{\omega_k}^Q - \omega_k| \le \delta_{\omega_k},\ k = 1, 2, 3, \tag{C.29}$$

$$|u_k^Q - u_k| \le \delta_{u_k},\ k = 1, 2, 3. \tag{C.30}$$

The quantization error of the quaternion can be expressed as

$$\boldsymbol{d}_q = \bar{\boldsymbol{q}}_{i,b} \otimes \boldsymbol{q}_{i,Q} = \begin{bmatrix} d_\eta \\ \boldsymbol{d}_\varepsilon \end{bmatrix} = \begin{bmatrix} \eta\eta^Q + \boldsymbol{\varepsilon}^\top \boldsymbol{\varepsilon}^Q \\ \eta\boldsymbol{\varepsilon}^Q - \eta^Q\boldsymbol{\varepsilon} - S(\boldsymbol{\varepsilon})\boldsymbol{\varepsilon}^Q \end{bmatrix}, \tag{C.31}$$

where $\boldsymbol{d}_\varepsilon$ is the quantization error and bounded by $\|\boldsymbol{d}_\varepsilon\| \le k_\varepsilon \|\boldsymbol{\delta}_\varepsilon\|$ from (C.28) and where $k_\varepsilon > 1$ is a positive constant, and d_η is bounded from the unity property of unit quaternion. If $\boldsymbol{q}^Q = \boldsymbol{q}$ and there is no quantization error, then $\boldsymbol{d}_q = [1\ 0\ 0\ 0]^\top$. The tracking error with the quantized value of the unit quaternion, $\boldsymbol{e}^Q$, is given by

$$\boldsymbol{e}^Q = \begin{bmatrix} \tilde{\eta}^Q \\ \tilde{\boldsymbol{\varepsilon}}^Q \end{bmatrix} = \begin{bmatrix} \eta_d\eta^Q + \boldsymbol{\varepsilon}_d^\top \boldsymbol{\varepsilon}^Q \\ \eta_d\boldsymbol{\varepsilon}^Q - \eta^Q\boldsymbol{\varepsilon}_d - S(\boldsymbol{\varepsilon}_d)\boldsymbol{\varepsilon}^Q \end{bmatrix}, \tag{C.32}$$

and can also be described by

$$\begin{aligned} \boldsymbol{e}^Q = \boldsymbol{q}_{d,b} \otimes \boldsymbol{q}_{b,Q} = \boldsymbol{e} \otimes \boldsymbol{d}_q &= \begin{bmatrix} \tilde{\eta} d_\eta - \tilde{\boldsymbol{\varepsilon}}^\top \boldsymbol{d}_\varepsilon \\ d_\eta \tilde{\boldsymbol{\varepsilon}} + \tilde{\eta}\boldsymbol{d}_\varepsilon + S(\tilde{\boldsymbol{\varepsilon}})\boldsymbol{d}_\varepsilon \end{bmatrix} \\ &= \begin{bmatrix} \tilde{\eta}^Q \\ \tilde{\boldsymbol{\varepsilon}} + (d_\eta - 1)\tilde{\boldsymbol{\varepsilon}} + \tilde{\eta}\boldsymbol{d}_\varepsilon + S(\tilde{\boldsymbol{\varepsilon}})\boldsymbol{d}_\varepsilon \end{bmatrix} \triangleq \begin{bmatrix} \tilde{\eta}^Q \\ \tilde{\boldsymbol{\varepsilon}} + \boldsymbol{d}_{\tilde{\varepsilon}} \end{bmatrix}, \end{aligned} \tag{C.33}$$

where the value of $\boldsymbol{d}_{\tilde{\varepsilon}}$ depends on the quantization error that is bounded by (C.28). If there is no quantization error, $\boldsymbol{d}_{\tilde{\varepsilon}} = \boldsymbol{0}$.
The quantized angular velocity $\boldsymbol{\omega}^Q$ is expressed as

$$\boldsymbol{\omega}^Q = \boldsymbol{\omega} + \boldsymbol{d}_\omega, \tag{C.34}$$

where $\boldsymbol{d}_\omega$ is the quantization error and is bounded by $\|\boldsymbol{d}_\omega\| \leq \|[\delta_{\omega_1}\ \delta_{\omega_2}\ \delta_{\omega_3}]^\top\| = \|\boldsymbol{\delta}_\omega\| \triangleq \delta_\omega$ from (C.29).
To propose a suitable control scheme, the quantized input $\boldsymbol{u}^Q(t)$ is decomposed into two parts

$$\boldsymbol{u}^Q(t) = \boldsymbol{u}(t) + \boldsymbol{d}_u(t), \tag{C.35}$$

where $\boldsymbol{d}_u$ is the quantization error of the input, which is bounded by $\|\boldsymbol{d}_u\| \leq \|[\delta_{u1}\ \delta_{u2}\ \delta_{u3}]^\top\| = \|\boldsymbol{\delta}_u\| \triangleq \delta_u$, from (C.30).
The adaptive controller is designed as

$$\boldsymbol{u}^Q(t) = Q(\boldsymbol{u}), \tag{C.36}$$

$$\boldsymbol{u}(t) = \boldsymbol{B}^{-1}\Big[-\boldsymbol{G}^Q\boldsymbol{z}_1^Q - \boldsymbol{C}_2\boldsymbol{z}_2^Q - \boldsymbol{\Phi}^Q\hat{\boldsymbol{\theta}} - \boldsymbol{\Psi}^Q - \boldsymbol{J}\Big(\boldsymbol{S}(\boldsymbol{\omega}^Q)\boldsymbol{R}_i^Q\boldsymbol{\omega}_d - \boldsymbol{R}_i^Q\dot{\boldsymbol{\omega}}_d - \bar{\boldsymbol{\alpha}}^Q\Big)\Big], \tag{C.37}$$

$$\dot{\hat{\boldsymbol{\theta}}} = \mathrm{Proj}\{\boldsymbol{\Gamma}\boldsymbol{\Phi}^Q\boldsymbol{z}_2^Q\}, \tag{C.38}$$

where $\mathrm{Proj}\{\cdot\}$ is the projection operator given in [34], and

$$\boldsymbol{z}_1^Q = \begin{bmatrix} 1 \mp \tilde{\eta}^Q \\ \tilde{\boldsymbol{\varepsilon}}^Q \end{bmatrix}, \tag{C.39}$$

$$\boldsymbol{z}_2^Q = \boldsymbol{\omega}_e^Q - \boldsymbol{\alpha}^Q, \tag{C.40}$$

$$\boldsymbol{G}(\boldsymbol{e}^Q)^\top = \begin{bmatrix} \pm(\tilde{\boldsymbol{\varepsilon}}^Q)^\top \\ \tilde{\eta}^Q\boldsymbol{I} + \boldsymbol{S}(\tilde{\boldsymbol{\varepsilon}}^Q) \end{bmatrix}, \tag{C.41}$$

$$\boldsymbol{\alpha}^Q = -\boldsymbol{C}_1\boldsymbol{G}^Q\boldsymbol{z}_1^Q = \mp\boldsymbol{C}_1\tilde{\boldsymbol{\varepsilon}}^Q, \tag{C.42}$$

$$\boldsymbol{\Psi}^Q = -\boldsymbol{S}(\boldsymbol{\omega}^Q)(\boldsymbol{J}\boldsymbol{\omega}^Q) - \boldsymbol{g}(\boldsymbol{q}^Q), \tag{C.43}$$

$$\boldsymbol{\Phi}^Q = \mathrm{diag}(-\boldsymbol{\omega}^Q), \tag{C.44}$$

$$\boldsymbol{g}(\boldsymbol{q}^Q) = -\boldsymbol{S}(\boldsymbol{r}_g^b)\boldsymbol{R}_i^Q\boldsymbol{f}_g^i, \tag{C.45}$$

$$\bar{\boldsymbol{\alpha}}^Q \triangleq \mp\frac{1}{2}\boldsymbol{C}_1\Big[\tilde{\eta}^Q\boldsymbol{I} + \boldsymbol{S}(\tilde{\boldsymbol{\varepsilon}}^Q)\Big]\boldsymbol{\omega}_e^Q, \tag{C.46}$$

$$\boldsymbol{\omega}_e^Q = \boldsymbol{\omega}^Q - \boldsymbol{R}_i^Q\boldsymbol{\omega}_d, \tag{C.47}$$

$$\boldsymbol{R}_i^Q = \boldsymbol{R}_b^Q\boldsymbol{R}_i^b, \tag{C.48}$$

where $\boldsymbol{R}_b^Q$ is the rotation due to the quantization error. It is noted that the following manipulation is used in (C.42).

$$\boldsymbol{G}^Q \boldsymbol{z}_1^Q = \pm\tilde{\boldsymbol{\varepsilon}}^Q - \tilde{\eta}^Q\tilde{\boldsymbol{\varepsilon}}^Q + \tilde{\boldsymbol{\varepsilon}}^Q\tilde{\eta}^Q + (\boldsymbol{S}(\tilde{\boldsymbol{\varepsilon}})^Q)^\top\tilde{\boldsymbol{\varepsilon}}^Q = \pm\tilde{\boldsymbol{\varepsilon}}^Q. \tag{C.49}$$

Remark 5. *The projection operator Proj$\{\cdot\}$ in* (C.38) *ensures that the estimates and estimation errors are nonzero and within known bounds, that is $\|\hat{\boldsymbol{\theta}}\| \leq k_\theta$ and $\|\tilde{\boldsymbol{\theta}}\| \leq k_\theta$, and has the property $-\tilde{\boldsymbol{\theta}}^\top\boldsymbol{\Gamma}^{-1}Proj(\boldsymbol{\tau}) \leq -\tilde{\boldsymbol{\theta}}^\top\boldsymbol{\Gamma}^{-1}\boldsymbol{\tau}$, which are helpful to guarantee the closed-loop stability.*

Remark 6. *Only the quantized output can be used in the designed controller. Since the quantized output is used in the design of the virtual controller $\boldsymbol{\alpha}^Q$ in* (C.42)*, the derivative of the virtual controller is discontinuous and can not be used in the design of the controller. Instead, a function $\bar{\boldsymbol{\alpha}}^Q$ is used in* (C.46)*, which is designed as if the output is not quantized.*

C.4 Stability Analysis

To analyze the closed-loop system stability, we first establish some preliminary results as stated in the following lemma.

Lemma 1. *The effects of output quantization are bounded by the following inequalities:*

$$\text{(i)}\ \boldsymbol{\omega}_e^Q \leq \boldsymbol{\omega}_e + \boldsymbol{\delta}_{\omega_e}, \tag{C.50}$$
$$\text{(ii)}\ \boldsymbol{z}_2^Q \leq \boldsymbol{z}_2 + \boldsymbol{\delta}_{z_2}, \tag{C.51}$$
$$\text{(iii)}\ \|\boldsymbol{G}\boldsymbol{z}_1 - \boldsymbol{G}^Q\boldsymbol{z}_1^Q\| \leq \delta_{z_1}, \tag{C.52}$$
$$\text{(iv)}\ \|\boldsymbol{R}_i^Q - \boldsymbol{R}_i^b\| \leq \delta_R, \tag{C.53}$$
$$\text{(v)}\ \|\boldsymbol{\Psi} - \boldsymbol{\Psi}^Q\| \leq \delta_{\Psi_1} + \delta_{\Psi_2}\|\boldsymbol{z}\|, \tag{C.54}$$
$$\text{(vi)}\ \|\boldsymbol{S}(\boldsymbol{\omega})\boldsymbol{R}_i^b - \boldsymbol{S}(\boldsymbol{\omega}^Q)\boldsymbol{R}_i^Q\| \leq \delta_{S_1} + \delta_{S_2}\|\boldsymbol{z}\|, \tag{C.55}$$
$$\text{(vii)}\ \|\bar{\boldsymbol{\alpha}}^Q - \dot{\boldsymbol{\alpha}}\| \leq \delta_{\bar{\alpha}_1} + \delta_{\bar{\alpha}_2}\|\boldsymbol{z}\|, \tag{C.56}$$
$$\text{(viii)}\ \|\boldsymbol{\Phi} - \boldsymbol{\Phi}^Q\| \leq \delta_\omega. \tag{C.57}$$

Proof: With the use of (C.8), (C.31), (C.34), (C.47), and (C.48), we have

$$\begin{aligned}
\boldsymbol{\omega}_e^Q &= \boldsymbol{\omega} + \boldsymbol{d}_\omega - \boldsymbol{R}_b^Q\boldsymbol{R}_i^b\boldsymbol{\omega}_d \\
&\leq \boldsymbol{\omega}_e + \Big(\Big[2d_\eta\boldsymbol{S}(\boldsymbol{d}_\varepsilon) - 2\boldsymbol{S}^2(\boldsymbol{d}_\varepsilon)^\top\Big]\boldsymbol{R}_i^b\boldsymbol{\omega}_d + \boldsymbol{\delta}_\omega\Big) \\
&\leq \boldsymbol{\omega}_e + \Big(2k_\varepsilon\Big[\boldsymbol{S}(\boldsymbol{\delta}_\varepsilon) + \boldsymbol{S}^2(\boldsymbol{\delta}_\varepsilon)\Big]\boldsymbol{R}_i^b\boldsymbol{\omega}_d + \boldsymbol{\delta}_\omega\Big) \triangleq \boldsymbol{\omega}_e + \boldsymbol{\delta}_{\omega_e}.
\end{aligned} \tag{C.58}$$

Using (C.28), (C.40), (C.42), and (C.50), we have

$$\begin{aligned}\boldsymbol{z}_2^Q &\le \boldsymbol{\omega}_e + \boldsymbol{\delta}_{\omega_e} \pm \boldsymbol{C}_1 \tilde{\boldsymbol{\varepsilon}}^Q \\ &\le \boldsymbol{\omega}_e + \boldsymbol{\delta}_{\omega_e} - \boldsymbol{\alpha} \pm \boldsymbol{C}_1 \boldsymbol{d}_{\tilde{\varepsilon}} \\ &\le \boldsymbol{z}_2 + (\boldsymbol{\delta}_{\omega_e} + \boldsymbol{C}_1 k_\varepsilon \boldsymbol{\delta}_\varepsilon) \triangleq \boldsymbol{z}_2 + \boldsymbol{\delta}_{z_2}. \end{aligned} \tag{C.59}$$

From the definition in (C.33) and the fact that $\boldsymbol{G}\boldsymbol{z}_1 = \pm\tilde{\boldsymbol{\varepsilon}}$ and $\boldsymbol{G}^Q \boldsymbol{z}_1^Q = \pm\tilde{\boldsymbol{\varepsilon}}^Q$, it is shown that

$$\|\boldsymbol{G}\boldsymbol{z}_1 - \boldsymbol{G}^Q \boldsymbol{z}_1^Q\| = \|\pm\tilde{\boldsymbol{\varepsilon}} - (\pm\tilde{\boldsymbol{\varepsilon}}^Q)\| \le \|\boldsymbol{d}_{\tilde{\varepsilon}}\| \le \|k_\varepsilon \boldsymbol{\delta}_\varepsilon\| \triangleq \delta_{z_1}. \tag{C.60}$$

By using (C.31) and (C.48) and the property of (C.8) and (C.9), we have

$$\begin{aligned}\|\boldsymbol{R}_i^Q - \boldsymbol{R}_i^b\| &= \|\boldsymbol{R}_b^Q \boldsymbol{R}_i^b - \boldsymbol{R}_i^b\| = \|(\boldsymbol{R}_b^Q - \boldsymbol{I})\boldsymbol{R}_i^b\| \\ &\le \|-2d_\eta \boldsymbol{S}(\boldsymbol{d}_\varepsilon) + 2\boldsymbol{S}^2(\boldsymbol{d}_\varepsilon)^\top\| \|\boldsymbol{R}_i^b\| \\ &\le 2\Big[k_\varepsilon \|\boldsymbol{\delta}_\varepsilon\| + k_\varepsilon^2 \|\boldsymbol{\delta}_\varepsilon\|^2\Big] \triangleq \delta_R. \end{aligned} \tag{C.61}$$

Using (C.4), (C.13), (C.31), (C.34), (C.43), (C.45), and (C.48), together with the property of (C.8) and Assumption 1, we have

$$\begin{aligned}\|\boldsymbol{\Psi} - \boldsymbol{\Psi}^Q\| &\le \|-\boldsymbol{S}(\boldsymbol{\omega})(\boldsymbol{J}\boldsymbol{\omega}) + \boldsymbol{S}(\boldsymbol{\omega}+\boldsymbol{d}_\omega)(\boldsymbol{J}(\boldsymbol{\omega}+\boldsymbol{d}_\omega)) + \boldsymbol{S}(\boldsymbol{r}_g^b)\boldsymbol{R}_i^b \boldsymbol{f}_g^i - \boldsymbol{S}(\boldsymbol{r}_g^b)\boldsymbol{R}_i^Q \boldsymbol{f}_g^i\| \\ &\le \Big[\lambda_{\max}(\boldsymbol{J})\Big(2k_{\omega_d}\|\boldsymbol{\delta}_\omega\| + \|\boldsymbol{\delta}_\omega\|^2\Big) + \|\boldsymbol{r}_g^b\|\delta_R mg\Big] + \Big[2\lambda_{\max}(\boldsymbol{J})\|\boldsymbol{\delta}_\omega\| k_{\omega_e}\Big]\|\boldsymbol{z}\| \\ &\triangleq \delta_{\Psi_1} + \delta_{\Psi_2}\|\boldsymbol{z}\|. \end{aligned} \tag{C.62}$$

By using (C.8), (C.27), (C.31), (C.34), (C.48) and (C.61), we have

$$\begin{aligned}\|\boldsymbol{S}(\boldsymbol{\omega})\boldsymbol{R}_i^b - \boldsymbol{S}(\boldsymbol{\omega}^Q)\boldsymbol{R}_i^Q\| &\le \|-\boldsymbol{S}(\boldsymbol{\omega})[-2d_\eta \boldsymbol{S}(\boldsymbol{d}_\varepsilon) + 2\boldsymbol{S}^2(\boldsymbol{d}_\varepsilon)^\top]\boldsymbol{R}_i^b - \boldsymbol{S}(\boldsymbol{d}_\omega)\boldsymbol{R}_i^Q\| \\ &\le \|\boldsymbol{\omega}\|\delta_R + \|\boldsymbol{\delta}_\omega\| \\ &\le (k_{\omega_d}\delta_R + \delta_\omega) + (k_{\omega_e}\delta_R)\|\boldsymbol{z}\| \triangleq \delta_{S_1} + \delta_{S_2}\|\boldsymbol{z}\|. \end{aligned} \tag{C.63}$$

By using (C.20), (C.26) (C.42), (C.46), and (C.50), we have

$$\begin{aligned}\|\bar{\boldsymbol{\alpha}}^Q - \dot{\boldsymbol{\alpha}}\| &= \|\frac{1}{2}\boldsymbol{C}_1\Big[\mp[\tilde{\eta}^Q \boldsymbol{I} + \boldsymbol{S}(\tilde{\boldsymbol{\varepsilon}}^Q)]\boldsymbol{\omega}_e^Q - [\mp[\tilde{\eta}\boldsymbol{I} + \boldsymbol{S}(\tilde{\boldsymbol{\varepsilon}})]]\boldsymbol{\omega}_e\Big]\| \\ &\le \frac{1}{2}\lambda_{\max}(\boldsymbol{C}_1)\Big(2\|\boldsymbol{\omega}_e\| + \|\boldsymbol{\delta}_{\omega_e}\|\Big) \\ &\le \lambda_{\max}(\boldsymbol{C}_1)(\frac{1}{2}\|\boldsymbol{\delta}_{\omega_e}\| + k_{\omega_e}\|\boldsymbol{z}\|) \triangleq \delta_{\bar{\alpha}_1} + \delta_{\bar{\alpha}_2}\|\boldsymbol{z}\|. \end{aligned} \tag{C.64}$$

From (C.5), (C.34) and (C.44), we have

$$\|\boldsymbol{\Phi} - \boldsymbol{\Phi}^Q\| \le \|\mathrm{diag}(-\boldsymbol{\omega}) - \mathrm{diag}(-\boldsymbol{\omega} - \boldsymbol{d}_\omega)\| \le \|\boldsymbol{\delta}_\omega\| = \delta_\omega. \tag{C.65}$$

We state our main results in the following theorem.

Theorem 1. *Considering the closed-loop adaptive system consisting of the plant* (C.1)-(C.2) *with output and input quantization satisfying the bounded properties* (C.28)-(C.30)*, the adaptive controller* (C.36)-(C.37)*, the update law* (C.38) *and Assumptions 1-3. If the gain matrices* $\boldsymbol{C}_1$ *and* $\boldsymbol{C}_2$ *and quantization parameters* $\boldsymbol{\delta}_\varepsilon$*,* $\boldsymbol{\delta}_\omega$ *and* $\boldsymbol{\delta}_u$ *are chosen to satisfy*

$$\frac{c_0}{2} - \delta_{V_1} \geq k > 0, \tag{C.66}$$

where c_0 *is the minimum eigenvalue of* $\boldsymbol{C}_0 = \min\{\boldsymbol{G}^\top \boldsymbol{C}_1 \boldsymbol{G}, \boldsymbol{C}_2\}$*,* k *is a positive constant, and* δ_{V_1} *is defined as*

$$\delta_{V_1} = \delta_{\Psi_2} + \delta_{S_2}\lambda_{\max}(\boldsymbol{J})k_{\omega_d} + \delta_{\bar{\alpha}_2}\lambda_{\max}(\boldsymbol{J}), \tag{C.67}$$

then, all signals in the closed loop system are ensured to be uniformly bounded. The error signals will converge to a compact set, i.e.,

$$\|\boldsymbol{z}(t)\| \leq \sqrt{\frac{\delta_Q}{k}}, \tag{C.68}$$

where

$$\delta_Q = \delta_{\theta_1} + \frac{1}{2c_0}\delta_{V_2}^2, \tag{C.69}$$

$$\delta_{\theta_1} = k_\theta \delta_\omega \|\boldsymbol{\delta}_{z_2}\| + k_\theta \|\boldsymbol{\delta}_{z_2}\| k_{\omega_d}, \tag{C.70}$$

$$\begin{aligned}\delta_{V_2} = {} & \lambda_{\max}(\boldsymbol{C}_2)\|\boldsymbol{\delta}_{z_2}\| + \delta_{z_1} + \delta_{\Psi_1} + \delta_{S_1}\lambda_{\max}(\boldsymbol{J})k_{\omega_d} + \delta_R\lambda_{\max}(\boldsymbol{J})k_{\dot{\omega}_d} + \delta_{\bar{\alpha}_1}\lambda_{\max}(\boldsymbol{J}) \\ & + \delta_{\theta_2} + \delta_{Bu},\end{aligned} \tag{C.71}$$

$$\delta_{\theta_2} = k_\theta \delta_\omega + k_\theta k_{\omega_e}\|\boldsymbol{\delta}_{z_2}\|. \tag{C.72}$$

Proof: Consider the Lyapunov function candidate

$$V(\boldsymbol{z}, \tilde{\boldsymbol{\theta}}, t) = \boldsymbol{z}_1^\top \boldsymbol{z}_1 + \frac{1}{2}\boldsymbol{z}_2^\top \boldsymbol{J}\boldsymbol{z}_2 + \frac{1}{2}\tilde{\boldsymbol{\theta}}^\top \boldsymbol{\Gamma}^{-1}\tilde{\boldsymbol{\theta}}. \tag{C.73}$$

Following (C.36)-(C.38), the derivative of (C.73) is given as

$$\begin{aligned}\dot{V} = {} & \boldsymbol{z}_1^\top \boldsymbol{G}^\top \boldsymbol{z}_2 - \boldsymbol{z}_1^\top \boldsymbol{G}^\top \boldsymbol{C}_1 \boldsymbol{G}\boldsymbol{z}_1 + \boldsymbol{z}_2^\top \Big[\boldsymbol{\Phi}\boldsymbol{\theta} + \boldsymbol{\Psi} + \boldsymbol{B}\boldsymbol{u}^Q + \boldsymbol{J}\Big(\boldsymbol{S}(\boldsymbol{\omega})\boldsymbol{R}_i^b\boldsymbol{\omega}_d - \boldsymbol{R}_i^b\dot{\boldsymbol{\omega}}_d - \dot{\boldsymbol{\alpha}}\Big)\Big] \\ & - \tilde{\boldsymbol{\theta}}^\top \boldsymbol{\Gamma}^{-1}\dot{\hat{\boldsymbol{\theta}}} \\ \leq {} & - \boldsymbol{z}_1^\top \boldsymbol{G}^\top \boldsymbol{C}_1 \boldsymbol{G}\boldsymbol{z}_1 - \boldsymbol{z}_2^\top \boldsymbol{C}_2 \boldsymbol{z}_2^Q + \boldsymbol{z}_2^\top (\boldsymbol{G}\boldsymbol{z}_1 - \boldsymbol{G}^Q \boldsymbol{z}_1^Q) + \boldsymbol{z}_2^\top (\boldsymbol{\Psi} - \boldsymbol{\Psi}^Q) \\ & + \boldsymbol{z}_2^\top \boldsymbol{J}(\boldsymbol{S}(\boldsymbol{\omega})\boldsymbol{R}_i^b - \boldsymbol{S}(\boldsymbol{\omega}^Q)\boldsymbol{R}_i^Q)\boldsymbol{\omega}_d + \boldsymbol{z}_2^\top \boldsymbol{J}\Big(\boldsymbol{R}_i^Q - \boldsymbol{R}_i^b\Big)\dot{\boldsymbol{\omega}}_d + \boldsymbol{z}_2^\top \boldsymbol{J}(\bar{\boldsymbol{\alpha}}^Q - \dot{\boldsymbol{\alpha}}) \\ & + \boldsymbol{z}_2^\top \boldsymbol{B}\boldsymbol{d}_u + \Big[\boldsymbol{z}_2^\top (\boldsymbol{\Phi}\boldsymbol{\theta} - \boldsymbol{\Phi}^Q\hat{\boldsymbol{\theta}}) - \tilde{\boldsymbol{\theta}}^\top \boldsymbol{\Phi}^Q \boldsymbol{z}_2^Q\Big].\end{aligned} \tag{C.74}$$

Using (C.30), the term containing the quantization error from the input in (C.74) satisfies

$$\boldsymbol{z}_2^\top \boldsymbol{B}\boldsymbol{d}_u \leq \|\boldsymbol{z}_2\|\|\boldsymbol{B}\|\delta_u \leq \delta_u\|\boldsymbol{B}\|\|\boldsymbol{z}\| \triangleq \delta_{Bu}\|\boldsymbol{z}\|. \tag{C.75}$$

By using (C.5), (C.34), (C.38), (C.44), (C.51), (C.27) and Assumption 2, the last terms in (C.74) satisfy the inequality

$$\begin{aligned}
\boldsymbol{z}_2^\top(\boldsymbol{\Phi}\boldsymbol{\theta} - \boldsymbol{\Phi}^Q\hat{\boldsymbol{\theta}}) - \tilde{\boldsymbol{\theta}}^\top\boldsymbol{\Phi}^Q\boldsymbol{z}_2^Q &= \boldsymbol{\theta}^\top\boldsymbol{\Phi}\boldsymbol{z}_2 - \boldsymbol{\theta}^\top\boldsymbol{\Phi}^Q\boldsymbol{z}_2 + \tilde{\boldsymbol{\theta}}^\top\boldsymbol{\Phi}^Q\boldsymbol{z}_2 - \tilde{\boldsymbol{\theta}}^\top\boldsymbol{\Phi}^Q\boldsymbol{z}_2^Q \\
&\leq \|\boldsymbol{\theta}\|\|\boldsymbol{\Phi} - \boldsymbol{\Phi}^Q\|\|\boldsymbol{z}_2\| + \|\tilde{\boldsymbol{\theta}}\|\|\boldsymbol{\Phi}^Q\|\|\boldsymbol{z}_2 - \boldsymbol{z}_2^Q\| \\
&\leq k_\theta\delta_\omega\|\boldsymbol{z}\| + k_\theta(\|\boldsymbol{\omega}\| + \|\boldsymbol{\delta}_\omega\|)\|\boldsymbol{\delta}_{z_2}\| \\
&\leq (k_\theta\delta_\omega\|\boldsymbol{\delta}_{z_2}\| + k_\theta\|\boldsymbol{\delta}_{z_2}\|k_{\omega_d}) + (k_\theta\delta_\omega + k_\theta k_{\omega_e}\|\boldsymbol{\delta}_{z_2}\|)\|\boldsymbol{z}\| \\
&\triangleq \delta_{\theta_1} + \delta_{\theta_2}\|\boldsymbol{z}\|.
\end{aligned} \tag{C.76}$$

By using Young's inequality, the properties in Lemma 1, (C.75), (C.76) and Assumption 1, (C.74) becomes

$$\begin{aligned}
\dot{V} \leq & -\boldsymbol{z}_1^\top\boldsymbol{G}^\top\boldsymbol{C}_1\boldsymbol{G}\boldsymbol{z}_1 - \boldsymbol{z}_2^\top\boldsymbol{C}_2\boldsymbol{z}_2 + \lambda_{\max}(\boldsymbol{C}_2)\|\boldsymbol{\delta}_{z_2}\|\|\boldsymbol{z}\| + \delta_{z_1}\|\boldsymbol{z}\| + \delta_{\Psi_1}\|\boldsymbol{z}\| + \delta_{\Psi_2}\|\boldsymbol{z}\|^2 \\
& + \delta_{S_1}\lambda_{\max}(\boldsymbol{J})k_{\omega_d}\|\boldsymbol{z}\| + \delta_{S_2}\lambda_{\max}(\boldsymbol{J})k_{\omega_d}\|\boldsymbol{z}\|^2 + \delta_R\lambda_{\max}(\boldsymbol{J})k_{\dot{\omega}_d}\|\boldsymbol{z}\| + \delta_{Bu}\|\boldsymbol{z}\| \\
& + \delta_{\bar{\alpha}_1}\lambda_{\max}(\boldsymbol{J})\|\boldsymbol{z}\| + \delta_{\bar{\alpha}_2}\lambda_{\max}(\boldsymbol{J})\|\boldsymbol{z}\|^2 + \delta_{\theta_1} + \delta_{\theta_2}\|\boldsymbol{z}\| \\
\leq & -c_0\|\boldsymbol{z}\|^2 + \delta_{\theta_1} + \delta_{V_2}\|\boldsymbol{z}\| + \delta_{V_1}\|\boldsymbol{z}\|^2 \\
\leq & -(\frac{c_0}{2} - \delta_{V_1})\|\boldsymbol{z}\|^2 + \delta_{\theta_1} + \frac{1}{2c_0}\delta_{V_2}^2 \\
\leq & -k\|\boldsymbol{z}\|^2 + \delta_Q < 0, \quad \forall\|\boldsymbol{z}\| > \sqrt{\delta_Q/k}.
\end{aligned} \tag{C.77}$$

From (C.73) and (C.77) and by applying the LaSalle-Yoshizawa theorem, it follows that $\boldsymbol{z}_1$, $\boldsymbol{z}_2$ and $\tilde{\boldsymbol{\theta}}$ are bounded and satisfy (C.68) under condition (C.66). From (C.37) and Lemma 1, it follows that the control input $\boldsymbol{u}$, where only the quantized output is measured, also is bounded. Thus, all signals in the closed loop system are bounded. Tracking of the desired reference signal is achieved, with a bounded tracking error given in (C.68).

Remark 7. *The value of δ_Q depends on the quantization parameters, and higher values of the quantization intervals will increase δ_Q. If there is no quantization, $\delta_Q = 0$. In principle, the quantization level can be chosen arbitrarily as long as the inequality* (C.66) *is satisfied, where δ_{V_1} depends on the quantization parameters $\boldsymbol{\delta}_\omega$ and $\boldsymbol{\delta}_\varepsilon$, and c_0 depends on the control design parameters. Therefore,* (C.66) *provides some insights on how to choose these quantization parameters.*

Next, we consider the case where external disturbances $\boldsymbol{\tau}_d$, assumed unknown

but bounded by $\|\boldsymbol{\tau}_d\| \leq k_{\tau_d}$, are present to the system, and the attitude dynamics are described by

$$\boldsymbol{J}\dot{\boldsymbol{\omega}} = \boldsymbol{\Psi}(\boldsymbol{q}, \boldsymbol{\omega}) + \boldsymbol{\Phi}(\boldsymbol{\omega})\boldsymbol{\theta} + \boldsymbol{B}\boldsymbol{u} + \boldsymbol{\tau}_d. \tag{C.78}$$

Corollary 1. *Let Assumptions 1-3 hold. Consider the closed-loop adaptive system consisting of the plant* (C.1), (C.78) *with output and input quantization satisfying the bounded properties* (C.28)-(C.30), *the adaptive controller* (C.36)-(C.37) *and the update law* (C.38). *Choosing the gain matrices* $\boldsymbol{C}_1$ *and* $\boldsymbol{C}_2$ *and quantization parameters* $\boldsymbol{\delta}_\varepsilon$, $\boldsymbol{\delta}_\omega$ *and* $\boldsymbol{\delta}_u$ *to satisfy* (C.66), *all signals in the closed loop system are ensured to be uniformly bounded. The error signals will converge to a compact set, i.e.,*

$$\|\boldsymbol{z}(t)\| \leq \sqrt{\frac{\delta_{Qdist}}{k}}, \tag{C.79}$$

where

$$\delta_{Qdist} = \delta_{\theta_1} + \frac{1}{2c_0}(\delta_{V_2} + k_{\tau_d})^2. \tag{C.80}$$

The proof follows along the same lines as the proof of Theorem 1.

Remark 8. *The proposed control method considered in this paper needs information of all system states, which is reasonable for rigid body systems where the attitude and the angular velocity are measured by sensors. If some states are not available, an observer will be needed. Another limitation is that only a bounded type of quantizer is considered in this paper, where the quantization error is bounded. The proposed method can be extended to compensate for unbounded quantization error caused by the logarithmic or hysteresis quantizers.*

C.5 Experimental Results

The proposed controller was tested on the Quanser Aero helicopter system, shown in Fig. C.3. This is a two-rotor laboratory equipment for flight control-based experiments. The setup has a horizontal position of the main thruster and a vertical position of the tail thruster, which resembles a helicopter with two propellers driven by two DC motors. This is a MIMO system with 2 DOF, and the helicopter can rotate around two axes where each input affects both rotational directions. The body fixed coordinate frame is visualized in Fig. C.3, and the inertial frame is coinciding with the body frame when $\boldsymbol{q} = [\pm 1\ 0\ 0\ 0]^\top$. The mathematical model is described by (C.1) and (C.2), and the parameters used for simulation and experiments are

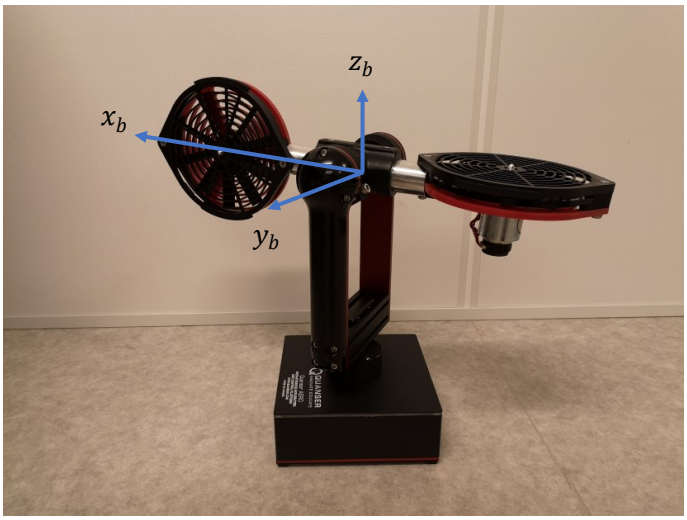

Figure C.3: Quanser Aero helicopter system with body coordinate frame.

Table C.1: Helicopter Parameters.

Symbol	Value	Units
$\boldsymbol{J}$	$\text{diag}(0.0218, 0.0217, 0.0218)$	kgm^2
m	1.075	kg
g	9.81	m/s^2
$\boldsymbol{r}_b^g$	$[0 \;\; 0 \;\; -0.0038]^\top$	m
$\boldsymbol{B}$	$\begin{bmatrix} 1 & 0 & 0 \\ 0 & 0.0011 & 0.0011 \\ 0 & -0.0014 & 0.00176 \end{bmatrix}$	Nm/V

shown in Table C.1. The initial states and estimated parameters were chosen as $\boldsymbol{q}(t_0) = [1\ 0\ 0\ 0]^\top$, $\boldsymbol{\omega}(t_0) = [0\ 0\ 0]^\top$ and $\hat{\boldsymbol{\theta}}(t_0) = [0\ 0.0070\ 0.0095]^\top$, where t_0 defines the start of experiment, and the design parameters were set to $\boldsymbol{C}_1 = 0.3\boldsymbol{I}$, $\boldsymbol{C}_2 = 0.15\boldsymbol{I}$ and $\boldsymbol{\Gamma} = 0.02\boldsymbol{I}$.

The objective was to track a sinusoidal signal where $r_d = 0$, $p_d = 40\pi/180 \sin(0.1\pi t)$, $y_d = 100\pi/180 \sin(0.05\pi t)$, given in Euler angles, that was converted to a quaternion, and also to track the angular velocities as given in (C.12), and see how the system was affected by quantization of the output and the input. The inputs have limits of $\pm$ 24 V. The length of the quantization interval for the outputs were chosen as $l_{\varepsilon_k} = l_{\omega_k} = 2/(2^R - 1),\ k = 1, 2, 3$, and for the inputs $l_{u_k} = 48/(2^R - 1),\ k = 1, 2, 3$, where R is number of bits transmitted in the communication. The system was tested with different values for R. The performance of the proposed control system was also tested subject to an external disturbance, where we set a fan to blow wind at the helicopter system.

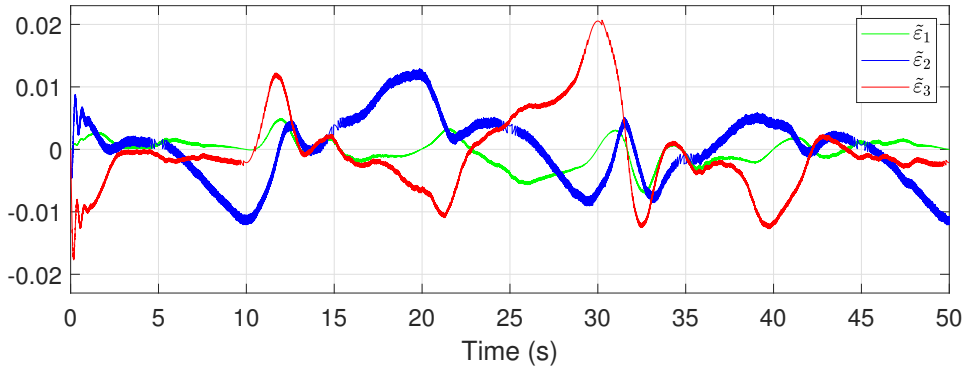

Figure C.4: Error in attitude $\tilde{\boldsymbol{\varepsilon}}$, from experiment, without quantization.

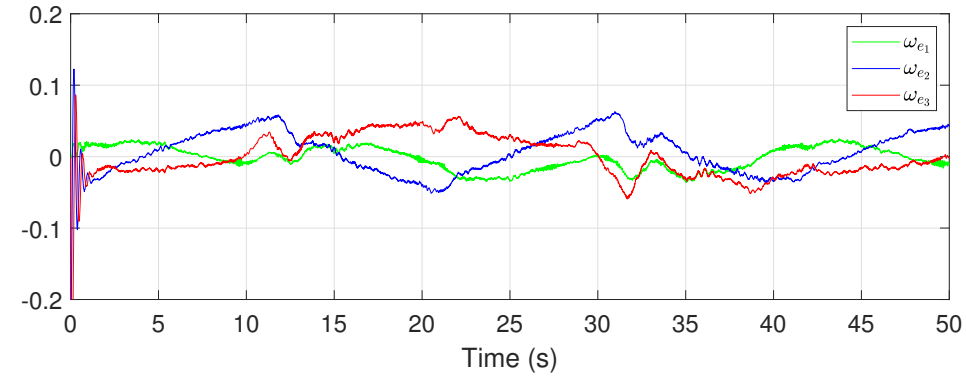

Figure C.5: Angular velocity error $\boldsymbol{\omega}_e$, from experiment, without quantization.

C.5.1 Results

The results from test without quantization are shown in Figs. C.4–C.6, showing the error in attitude $\tilde{\boldsymbol{\varepsilon}}$, the error in angular velocity $\boldsymbol{\omega}_e$, and the input $\boldsymbol{u}$, respectively. From Figs. C.4 and C.5, tracking of the desired reference signals are achieved and the tracking errors are bounded. The value of $\tilde{\varepsilon}_{(\cdot)}$ is within $[-0.02 \quad +0.02]$, that corresponds to an error of about ± 0.04 rad or ± 2.3 deg in Euler angles. The input signal in Fig. C.6 is also bounded.

The system was then tested with quantized output and input. We tested with different values for R, and plots for quantization levels chosen as $R = 8$ for the output, and $R = 6$ for the input, are shown in Figs. C.7–C.11, showing the outputs $\boldsymbol{q}^Q$ and $\boldsymbol{\omega}^Q$, the error in attitude $\tilde{\boldsymbol{\varepsilon}}^Q$, the error in angular velocity $\boldsymbol{\omega}_e^Q$ and the input $\boldsymbol{u}^Q$, respectively. The desired states are shown with a dotted line, and measured values from tests on the helicopter model are shown with a solid line. The results show that tracking is achieved and that all signals are uniformly bounded, in accordance with the findings of Theorem 1.

Next, an external disturbance was added to the system in form of wind, where the input and outputs were quantized. Figs. C.12–C.14 show the attitude error $\tilde{\boldsymbol{\varepsilon}}^Q$, the angular velocity error $\boldsymbol{\omega}_e^Q$ and the input $\boldsymbol{u}^Q$, respectively. As can be seen from

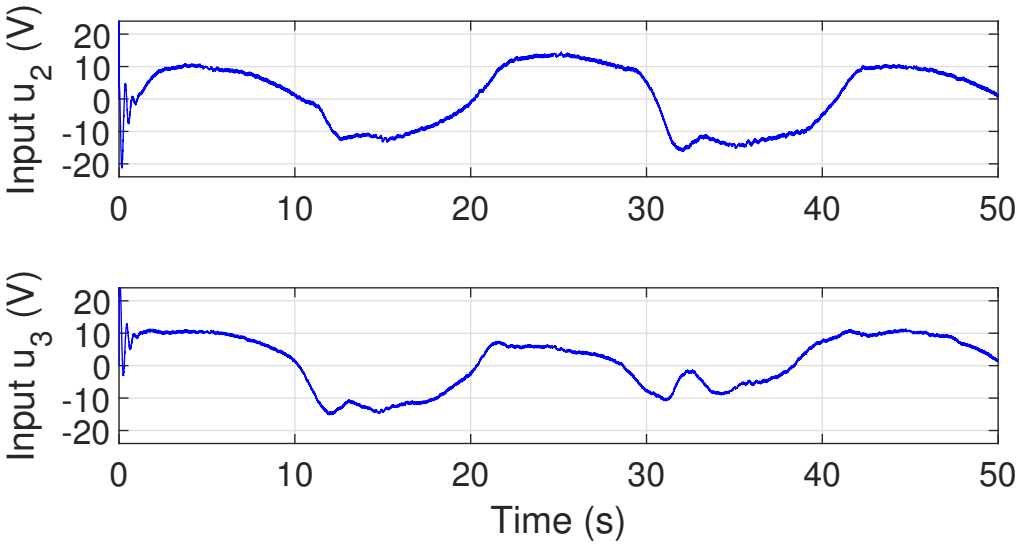

Figure C.6: Inputs u_2 and u_3 from experiment, without quantization.

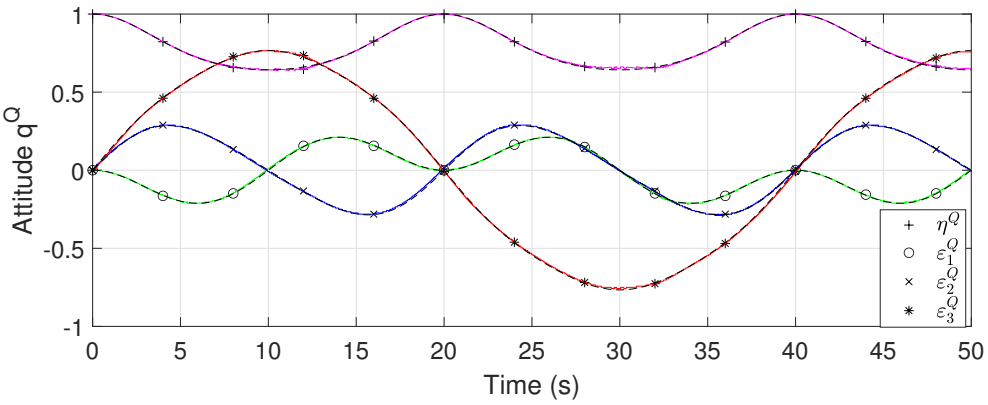

Figure C.7: Attitude $\boldsymbol{q}^Q$ from experiment with quantization.

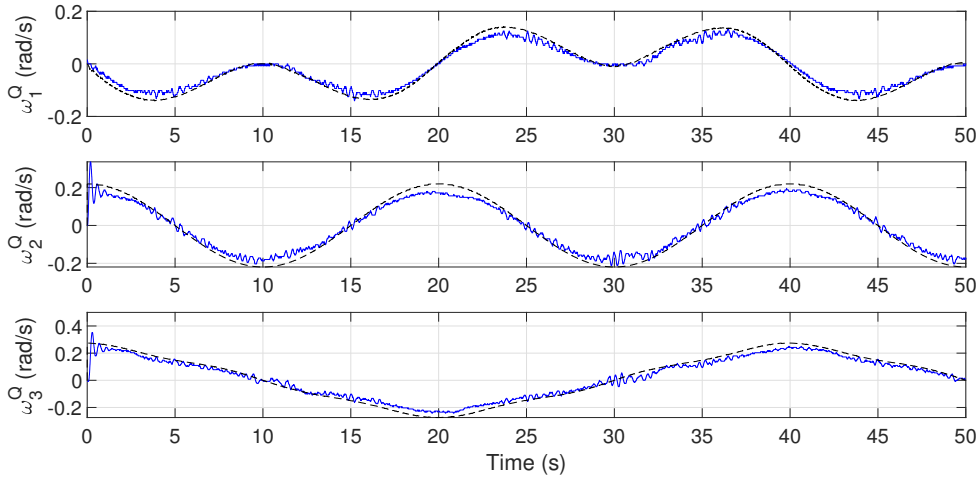

Figure C.8: Angular velocity $\boldsymbol{\omega}^Q$ from experiment with quantization.

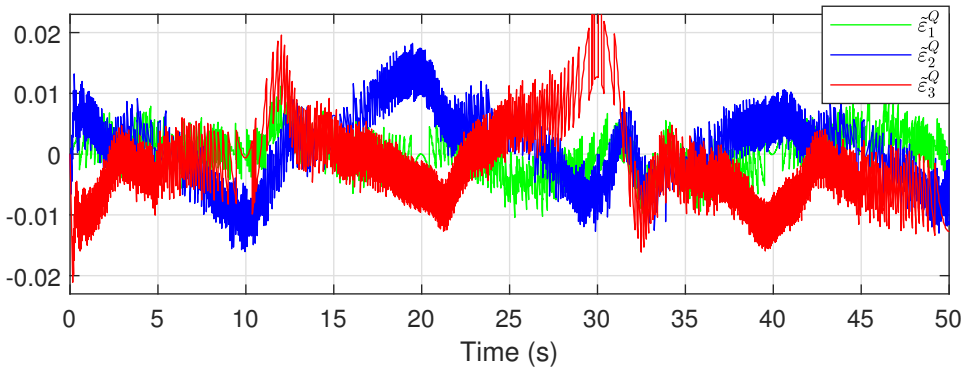

Figure C.9: Error in attitude $\tilde{\boldsymbol{\varepsilon}}^Q$ from experiment with quantization.

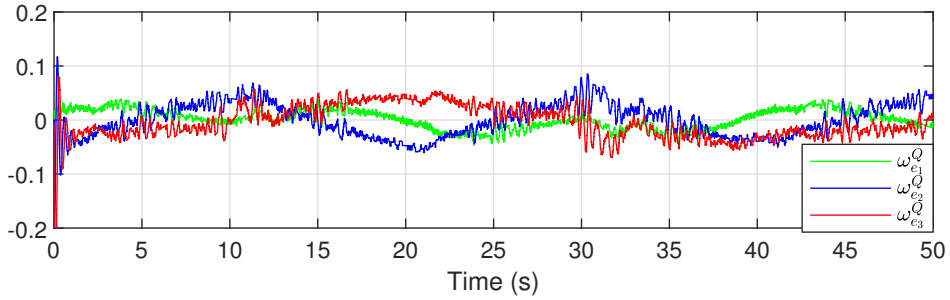

Figure C.10: Angular velocity error $\boldsymbol{\omega}_e^Q$ from experiment with quantization.

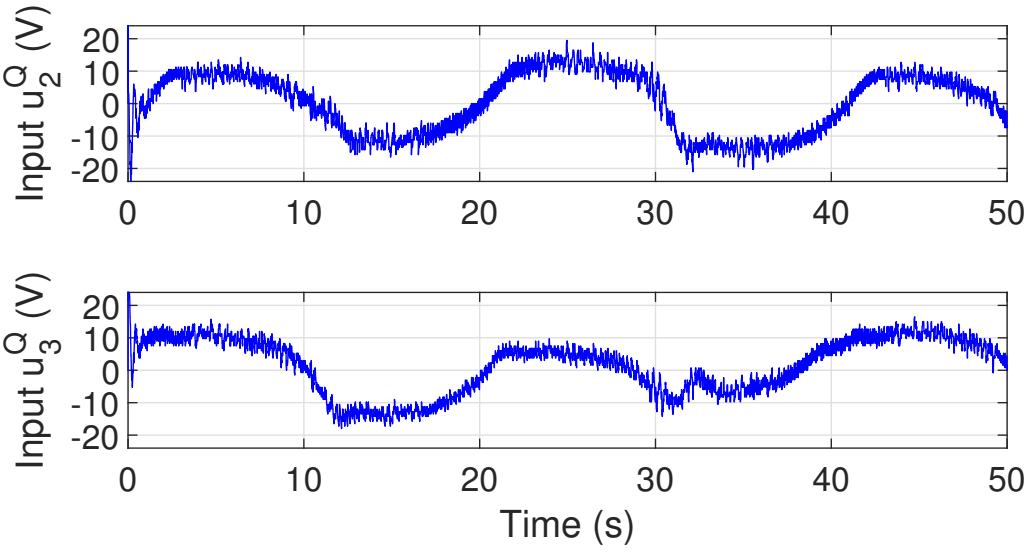

Figure C.11: Inputs u_2^Q and u_3^Q from experiment with quantization.

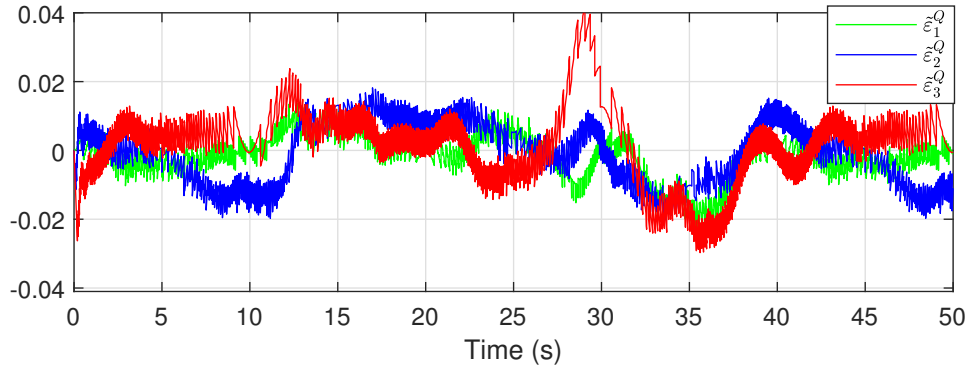

Figure C.12: Error in attitude $\tilde{\boldsymbol{\varepsilon}}^Q$ from experiment with external disturbance.

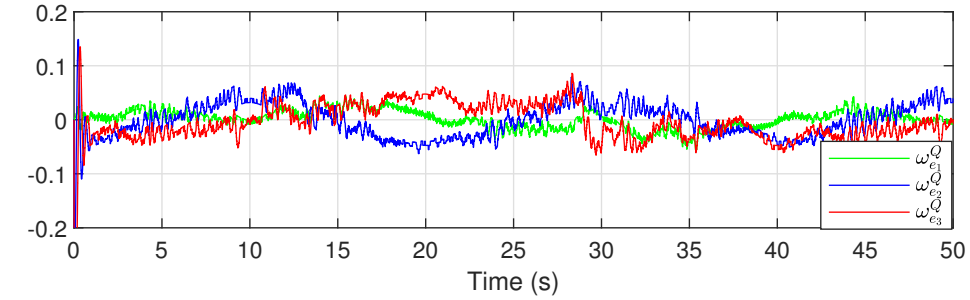

Figure C.13: Angular velocity error $\boldsymbol{\omega}_e^Q$ from experiment with external disturbance.

the plots, the errors in attitude and angular velocity are kept close to zero during tracking of the reference signals in presence of an external disturbance.

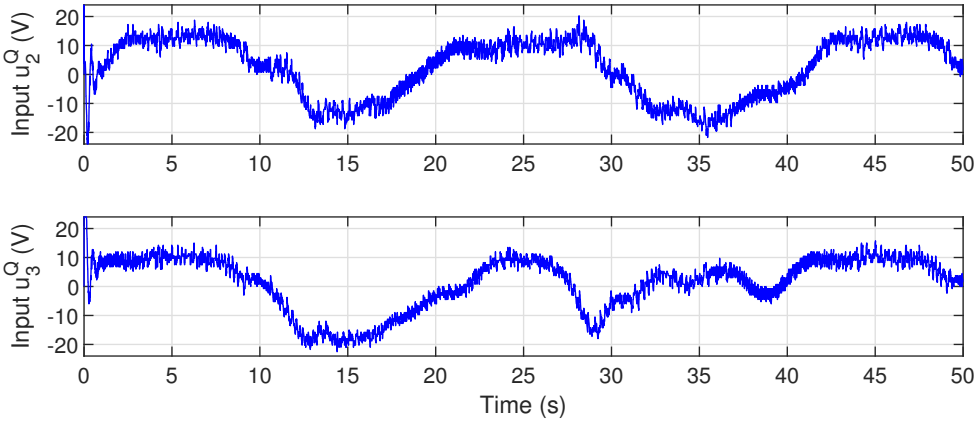

Figure C.14: Inputs u_2^Q and u_3^Q from experiment with external disturbance.

Table C.2: Tracking error for different quantization levels

z_{track} $\times 10^{-4}$	**Output $\boldsymbol{\varepsilon}^Q$, $\boldsymbol{\omega}^Q$ with $l_s = 2/(2^R-1)$**				
Input $\boldsymbol{u}^Q$ with $l_u = 48/(2^R-1)$	R	8	9	10	cont.
	6	49	51	38	38
	7	43	40	37	40
	8	45	40	39	45
	9	45	40	40	43
	10	47	40	39	38
	cont	43	35	34	35

Table C.3: Total energy use for different quantization levels

u_{total}	**Output $\boldsymbol{\varepsilon}^Q$, $\boldsymbol{\omega}^Q$ with $l_s = 2/(2^R-1)$**				
Input $\boldsymbol{u}^Q$ with $l_u = 48/(2^R-1)$	R	8	9	10	cont.
	6	8042	8168	7884	7945
	7	7881	7935	7897	8023
	8	8095	7895	7898	8017
	9	8055	7857	7959	8034
	10	8121	7970	7892	7899
	cont	8147	7854	7767	7980

C.5.2 Comparing Results

To compare the results with and without quantization, the total tracking error, z_{track}, and the total use of energy, u_{total}, were measured, where

$$z_{\text{track}} = \int_{t_0}^{t_f} (\tilde{\boldsymbol{\varepsilon}}^Q)^\top \tilde{\boldsymbol{\varepsilon}}^Q d\tau, \;\; u_{\text{total}} = \int_{t_0}^{t_f} (\boldsymbol{u}^Q)^\top \boldsymbol{u}^Q d\tau, \tag{C.81}$$

where t_0 and t_f define start and end of experiment, respectively. The experiments were run for 50 s. The tracking error and total use of energy for different values of R are shown in Tables C.2 and C.3.

From Table C.2, it is observed that for higher quantization levels, the tracking error increases. This is according to the findings of Theorem 1. For high values of R, i.e. for small quantization intervals, the system does not show a big difference in performance compared to when using continuous signals. A lower value for R is also possible, and will require less data transmission, but with the cost of higher tracking error, and also with more chattering for the input. The system is more affected by quantization of the output than of the input in terms of tracking error. Table C.4 compares the tracking error and total use of energy when an external disturbance was added. The quantization levels were chosen as $R = 8$ for the output, and $R = 6$ for the input. From this experiment, the tracking error increased when a disturbance was introduced, in accordance with the findings of Corollary 1, and also the total use of energy increased. By choosing a small quantization interval, the communication

Table C.4: Tracking error and total use of energy with and without external disturbance

	No disturbance		**External disturbance**	
	z_{track} $\times 10^{-4}$	u_{total}	z_{track} $\times 10^{-4}$	u_{total}
Continuous signals	35	7980	97	9241
Quantized signals	49	8042	119	9699

burden over a network can be reduced, and still achieve a good performance.

C.6 Conclusion

In this article, an adaptive backstepping control scheme is developed for attitude tracking using quaternions where the output and the input are quantized. The quantizer considered satisfies a bounded condition and so the quantization error is bounded. The full state is considered in the stability analysis, and with the use of constructed Lyapunov functions, all signals in the closed loop system are shown to be uniformly bounded and also tracking of a given reference signal is achieved. Experiments on a 2-DOF helicopter system supports the proof, where a uniform quantizer is tested for the system. As illustrated in the experiment, it is possible to reduce the communication burden over the network by including quantization, where a suitable quantization level must be chosen, depending on the performance requirement for the application.

References – Paper C

[1] J. T.-Y. Wen and K. Kreutz-Delgado, "The attitude control problem," *IEEE Transactions on Automatic Control*, vol. 36, no. 10, pp. 1148–1162, 1991.

[2] R. Schlanbusch, A. Loria, R. Kristiansen, and P. J. Nicklasson, "PD+ attitude control of rigid bodies with improved performance," in *49th IEEE Conference on Decision and Control*, 2010.

[3] N. A. Chaturvedi, A. K. Sanyal, and N. H. McClamroch, "Rigid-body attitude control," *IEEE Control Systems Magazine*, vol. 31, no. 3, pp. 30–51, 2011.

[4] C. G. Mayhew, R. G. Sanfelice, and A. R. Teel, "Quaternion-based hybrid control for robust global attitude tracking," *IEEE Transactions on Automatic Control*, vol. 56, no. 11, pp. 2555–2566, 2011.

[5] R. Schlanbusch, "Control of rigid bodies," Ph.D. dissertation, NTNU - Norwegian University of Science and Technology, 2012.

[6] T. Lee, "Robust adaptive attitude tracking on SO(3) with an application to a quadrotor UAV," *IEEE Transactions on Control Systems Technology*, vol. 21, no. 5, pp. 1924–1930, 2013.

[7] A. Benallegue, Y. Chitour, and A. Tayebi, "Adaptive attitude tracking control of rigid body systems with unknown inertia and gyro-bias," *IEEE Transactions on Automatic Control*, vol. 63, no. 11, pp. 3986–3993, 2018.

[8] T. Wang and J. Huang, "Leader-following adaptive consensus of multiple uncertain rigid body systems over jointly connected networks," *Unmanned Systems*, vol. 08, no. 02, pp. 85–93, 2020.

[9] T. S. Andersen and R. Kristiansen, "Adaptive backstepping control for a fully-actuated rigid-body in a dual-quaternion framework," in *2019 IEEE 58th Conference on Decision and Control (CDC)*, 2019.

[10] T. I. Fossen, *Marine Control Systems: Guidance, Navigation, and Control of Ships, Rigs and Underwater Vehicles*. Trondheim, Norway: Marine Cybernetics AS, 2002.

[11] F. Chen, R. Jiang, K. Zhang, B. Jiang, and G. Tao, "Robust backstepping sliding-mode control and observer-based fault estimation for a quadrotor uav," *IEEE Transactions on Industrial Electronics*, vol. 63, no. 6, pp. 5044–5056, 2016.

[12] S. M. Schlanbusch and J. Zhou, "Adaptive backstepping control of a 2-dof helicopter," in *Proceedings of the IEEE 7th International Conference on Control, Mechatronics and Automation*, 2019, pp. 210–215.

[13] Y. Yan and S. Yu, "Sliding mode tracking control of autonomous underwater vehicles with the effect of quantization," *Ocean Engineering*, vol. 151, pp. 322–328, 2018.

[14] X. Liang, Y. Fang, N. Sun, and H. Lin, "Nonlinear hierarchical control for unmanned quadrotor transportation systems," *IEEE Transactions on Industrial Electronics*, vol. 65, no. 4, pp. 3395–3405, 2018.

[15] A. E. Jimenez-Cano, P. J. Sanchez-Cuevas, P. Grau, A. Ollero, and G. Heredia, "Contact-based bridge inspection multirotors: Design, modeling, and control considering the ceiling effect," *IEEE Robotics and Automation Letters*, vol. 4, no. 4, pp. 3561–3568, 2019.

[16] C. Sampedro, A. Rodriguez-Ramos, H. Bavle, A. Carrio, P. de la Puente, and P. Campoy, "A fully-autonomous aerial robot for search and rescue applications in indoor environments using learning-based techniques," *Journal of Intelligent & Robotic Systems*, vol. 95, no. 2, pp. 601–627, 2018.

[17] J. Yan, J. Gao, X. Yang, X. Luo, and X. Guan, "Position tracking control of remotely operated underwater vehicles with communication delay," *IEEE Transactions on Control Systems Technology*, vol. 28, no. 6, pp. 2506–2514, 2020.

[18] S. Tatikonda and S. Mitter, "Control under communication constraints," *IEEE Transactions on Automatic Control*, vol. 49, no. 7, pp. 1056–1068, 2004.

[19] M. Fu and L. Xie, "The sector bound approach to quantized feedback control," *IEEE Transactions on Automatic Control*, vol. 50, no. 11, pp. 1698–1711, 2005.

[20] C. D. Persis, "Robust stabilization of nonlinear systems by quantized and ternary control," *Systems & Control Letters*, vol. 58, no. 8, pp. 602–608, 2009.

[21] T. Hayakawa, H. Ishii, and K. Tsumaru, "Adaptive quantized control for nonlinear uncertain systems," *Systems & Control Letters*, vol. 58, no. 9, pp. 625–632, 2009.

[22] H. Sun, N. Hovakimyan, and T. Basar, "$\mathcal{L}_1$ adaptive controller for uncertain nonlinear multi-input multi-output systems with input quantization," *IEEE Transactions on Automatic Control*, vol. 57, no. 3, pp. 565–578, 2012.

[23] J. Zhou, C. Wen, and G. Yang, "Adaptive backstepping stabilization of nonlinear uncertain systems with quantized input signal," in *IEEE Transactions on Automatic Control*, vol. 59, no. 2, 2014, pp. 460–464.

[24] J. Zhou, C. Wen, and W. Wang, "Adaptive control of uncertain nonlinear systems with quantized input signal," *Automatica*, vol. 95, pp. 152–162, 2018.

[25] Y. Li and G. Yang, "Adaptive asymptotic tracking control of uncertain nonlinear systems with input quantization and actuator faults," *Automatica*, vol. 72, pp. 177–185, 2016.

[26] A. Selivanov, A. Fradkov, and D. Liberzon, "Adaptive control of passifiable linear systems with quantized measurements and bounded disturbances," *Systems and Control Letters*, vol. 88, pp. 62–67, 2016.

[27] J. Zhou, C. Wen, W. Wang, and F. Yang, "Adaptive backstepping control of nonlinear uncertain systems with quantized states," *IEEE Transactions on Automatic Control*, vol. 64, no. 11, pp. 4756–4763, 2019.

[28] R. Sun, A. Shan, C. Zhang, J. Wu, and Q. Jia, "Quantized fault-tolerant control for attitude stabilization with fixed-time disturbance observer," *Journal of Guidance, Control, and Dynamics*, vol. 44, no. 2, pp. 449–455, 2021.

[29] B. Huang, B. Zhou, S. Zhang, and C. Zhu, "Adaptive prescribed performance tracking control for underactuated autonomous underwater vehicles with input quantization," *Ocean Engineering*, vol. 221, 2021.

[30] S. M. Schlanbusch and J. Zhou, "Adaptive backstepping control of a 2-DOF helicopter system with uniform quantized inputs," in *IECON 2020 The 46th Annual Conference of the IEEE Industrial Electronics Society*, 2020, pp. 88–94.

[31] Y. Wang, L. He, and C. Huang, "Adaptive time-varying formation tracking control of unmanned aerial vehicles with quantized input," *ISA Transactions*, vol. 85, pp. 76–83, 2019.

[32] L. Xing, C. Wen, Y. Zhu, H. Su, and Z. Liu, "Output feedback control for uncertain nonlinear systems with input quantization," *Automatica*, vol. 65, pp. 191–202, 2015.

[33] O. Egeland and J. T. Gravdahl, *Modeling and Simulation for Automatic Control*. Marine Cybernetics AS, 2003.

[34] M. Krstić, I. Kanellakopoulos, and P. Kokotović, *Nonlinear and Adaptive Control Design*. John Wiley & Sons, Inc., 1995.